Eur Respir J 1998; 11: 1392–1404
DOI: 10.1183/09031936.98.11061392

European Respiratory Journal
ISSN 0903 - 1936

REVIEW

Magnetic resonance (MR) imaging of the chest: state-of-the-art

R.C. Bittner, R. Felix

Magnetic resonance (MR) imaging of the chest: state-of-the-art. R.C. Bittner, R. Felix. ©ERS Journals Ltd 1998.

ABSTRACT: To date, magnetic resonance (MR) is established as an imaging modality in the diagnosis of chest diseases. Because of its excellent distinction of vessels and soft tissue, MR can be performed as the primary imaging procedure before computed tomography in patients with suspected vascular lesions, mediastinal masses, hilar lesions, and pathological changes of the pleura and the chest wall. In these cases, MR is able to provide all the necessary diagnostic information. In other patients, a limited number of MR images may be helpful in cases of equivocal or confusing CT or clinical findings. More detailed information can be obtained, using surface coils or special imaging sequences, *i.e*. high resolution MR images of the pleura or angiographic images of mediastinal and pulmonary vasculature.

From a clinical viewpoint, the most important task for thoracic magnetic resonance nowadays is the pretherapeutic evaluation of intrathoracic masses, the differential diagnosis of benign *versus* malignant lesions, and the accurate documentation of tumour extent in malignancies including three-dimensional-display to improve surgical or radiation planning. Future directions in thoracic magnetic resonance will be predominantly influenced by postprocessing approaches, specialized imaging techniques, and magnetic resonance-guided interventional applications.

Eur Respir J 1998; 11: 1392–1404.

Strahlen- und Poliklinik, Charité, Campus Virchow-Klinikum, Medical Faculty, Humboldt-University, Berlin, Germany.

Correspondence: R.C. Bittner
Strahlen- und Poliklinik
Charité, Campus Virchow-Klinikum, HU Berlin
Augustenburger Platz 1
D-13353 Berlin
Germany
Fax: 49 30 450 57900

Keywords: Contrast material
magnetic resonance angiography
magnetic resonance imaging
mediastinum
pleura
thorax

Received: May 27 1997
Accepted after revision January 20 1998

Since the early 1980s, magnetic resonance (MR) imaging has been used for the evaluation of chest diseases [1–43]. In the late 1980s, MR gained ground against the established computed tomography (CT), but later lost this due to the introduction of spiral CT [4, 6, 20, 34, 44–52]. However, the main advantages of MR over CT are its ability to perform multiplanar imaging and the excellent soft tissue contrast. Another advantage is the depiction of vascular structures without use of contrast material. In recent years MR has been accepted beside the CT, and in selected cases even as a primary diagnostic tool. Nevertheless, many applications of this imaging technique remain the subject of investigation; however, enough is known today to suggest appropriate clinical indications for thoracic MR.

Technique

In contrast to other applications, the image quality of thoracic MR depends to a large extent on technical and examiner conditions and experiences, because it is different from MR examinations of other organs or regions. For most chest MR exams, excellent electrocardiogram (ECG)-gating has to be achieved and prior patient's compliance is required.

An advantage of MR over CT is the direct imaging in the multiple planes of choice, which can provide information that is not available on transaxial images. Structures oriented longitudinally from cranial to caudal or oblique can be imaged along their axis, such as the trachea, oesophagus, superior vena cava, aorta or the brachial plexus. Imaging in a second plane reduces the possibility of misinterpretation of findings as a result of partial volume effects, *i.e*. in the area of the aorto-pulmonary window, the subcarinal region, and in pathological processes near the diaphragm or the lung apices. The most essential parameters of the predominantly used imaging methods in thoracic MR [24, 41] shall be briefly addressed: basically, there are two different imaging parameters, T1- and T2-weighting, which lead to different signal intensities (SI) of different tissues on MR images. Thus, MR images are called T1- or T2-weighted images, respectively. Fat as well as MR contrast material are displayed with increased SI (bright) in T1-weighted images. Water, fluid, and structures with high water content present with low SI (dark) in T1-weighted images. The T2-weighted image shows water with increased SI and the same applies to changes with a high water content, *e.g*. inflammatory changes, the majority of tumours, and nearly all pathological tissues (table 1).

For clinical use, T1-weighted images allow for excellent soft tissue contrast-resolution and provide the best spatial resolution for topographic evaluation. T2-weighted images are necessary for the detection and assessment of the extent of pathological changes with increased SI.

To date, in a routine chest examination (1.0–1.5 T magnetic field strength), a multi-slice (up to 32 sections), ECG-gated, T1-weighted spin-echo sequence is generated within 3–7 min, in the transaxial and either coronal/sagittal or oblique plane, respectively [19]. The slice thickness should be 3–8 mm, the field-of-view (FOV) may vary from 18–40 cm,

Table 1. – Characteristic signal intensity (SI) patterns of different tissues

Process	T1-weighted	T2-weighted	Comment
Simple cyst	Low	High	Homogeneous, sharply defined
Bronchogenic cyst	Low-medium-high	High-very high	SI dependent on protein content, fluid level possible
Seroma	Low	High	Like cysts
Abscess	Low-medium	High	Heterogeneous, ill-defined, often fluid level
Lipoma	High	Medium-high	Sometimes brighter than normal fat
Neurinoma, schwannoma	Low-medium	Medium-high	Heterogeneous, often centrally high SI on T2
Thymoma	Low-medium	Medium	Homogeneous, sharply defined
Malignant lymphoma (Hodgkin's)	Low-medium	Low-high	Heterogeneous, high SI of tumour interspersed with low SI of fibrosis
Malignant lymphoma (non-Hodgkin's)	Low-medium	High	Mostly homogeneous blurred margins
Bronchogenic carcinoma	Low-medium	Medium-high	Mostly heterogeneous, blurred margins
Arteriovenous malformation	Very low-signal void	Medium-low	Appearance dependent on flow
Obstructive atelectasis	Low-medium	High	
Non-obstructive atelectasis	Low-medium	Low	
Pulmonary secretions	Low	High	
Alveolar proteinosis	Medium-low	Medium-low	
Haemorrhage			
Acute	Low	Low-medium	Homogeneous
Subacute	Medium-high	High	Heterogeneous fluid, fluid level
Chronic	Low	Medium-high	Homogeneous with dark rim
Blood clot			
Acute	Medium	Medium-high	Magnetic
Chronic	Medium	Medium-low	Susceptibility effects

and the spatial resolution is approximately 1–2 mm. In diseases of the pleura and the chest wall or pulmonary processes near or in contact with the pleura, surface coils may be used with reduction of the FOV down to 8 cm, allowing for an excellent spatial resolution of 0.3 mm [11]. This may be followed by a fast non-gated T2-weighted sequence in one plane corresponding to the T1-weighted images, for up to 26 images within 4–6 min [11, 41]. The T2-weighted images display suspected increased SI and are helpful in showing fluid collection, distinguishing tumour from fibrosis, or chest wall musculature, and identifying flow phenomena, but the anatomical resolution is poor.

Several software programs have been introduced to eliminate flow, breathing and motion artifacts. In our experience, presaturation of the anterior chest wall provides the most effective suppression of diminishing artifacts in lung

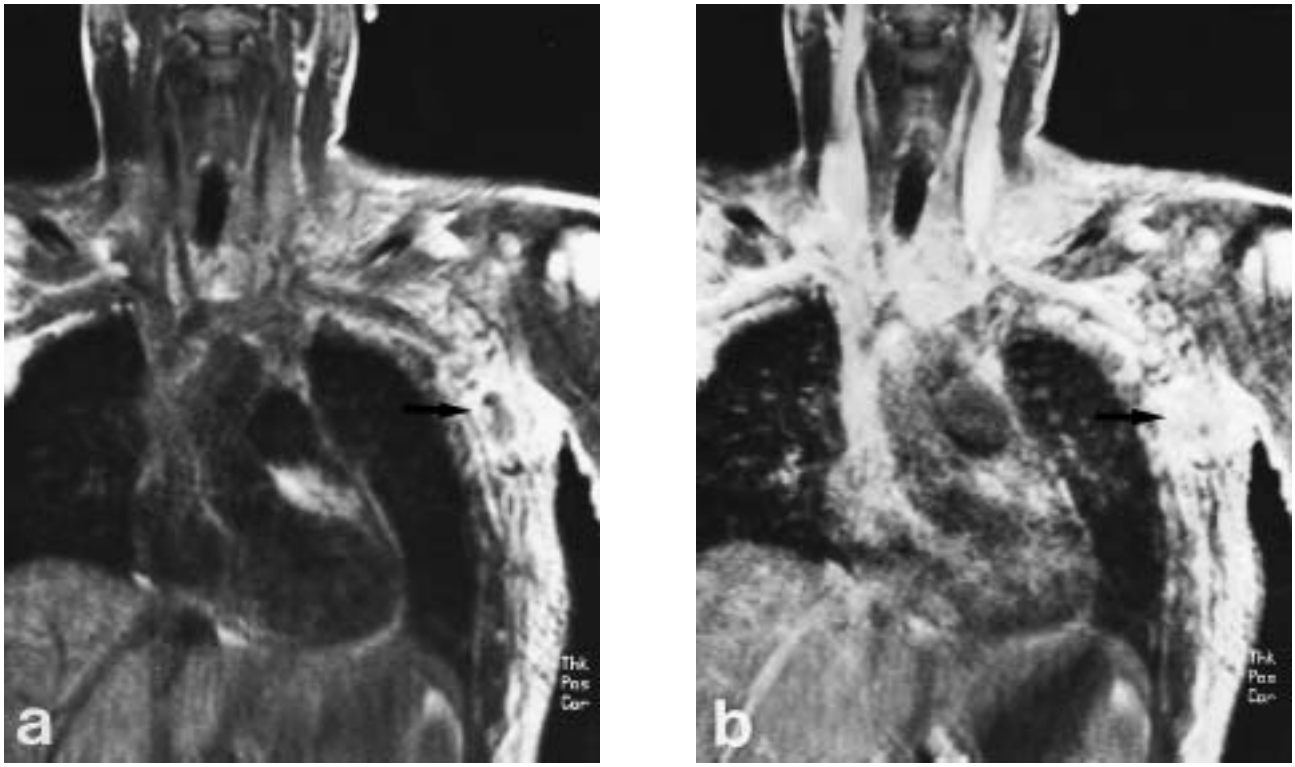

Fig. 1. – Magnetic resonance imaging of a severely ill patient with mediastinitis and extended soft tissue phlegmone spreading from an axillary abscess (arrows). Coronal T1-weighted a) pre and b) postcontrast images show intense and extended contrast enhancement within the cervical, chest wall, neck, and mediastinal soft tissue. Fast images, pre and postcontrast within 2.5 min.

and mediastinal MR exams [12, 19]. Postprocessing programs can significantly improve the image quality [4, 5, 35, 41].

The use of contrast material in thoracic MR is still a matter of controversy. Contrast-enhanced MR may be useful in pulmonary and mediastinal masses to detect necrosis or fibrosis [3–5, 7–13, 19, 20, 23, 28], and differential diagnosis may be improved [9–13]. Especially in pleural diseases, in pulmonary processes adjacent to the pleura, and in chest wall changes, contrast-enhanced T1-weighted MR has been found to be advantageous because of its improved ability to delineate lesions from normal structures [8–11]. For imaging vascular structures and diagnosing cardiac and vascular abnormalities, fast or dynamic imaging techniques are most valuable. Fast dynamic (Cine-) MR may show flowing blood with a very intense signal, and ECG-gated, flow phenomena and cardiac function can be demonstrated to great advantage [16, 23, 35, 41, 43]. Subsecond sequences allow for cine-images of the breathing lung [21].

Rapid acquisition of spin-echo images may produce good T1-weighted images during a breath-hold, so that contrast-enhanced dynamic studies are feasible [1, 7, 23, 28, 29]. Thus, even emergency care patients can be examined within few minutes prior to and after contrast (fig. 1).

Respiratory gating significantly increases the examination time, is difficult to combine with ECG-gating and is generally not used in clinical imaging [2, 19, 33, 36]. Technical progress has resulted in postprocessing procedures with significant improvement of image quality without prolongation of the patient's examination time and allow for vivid preoperative three-dimensional (3D)-display of thoracic masses [41].

Contraindications

There are no documented, lasting, harmful effects from MR. In high field strength magnets, radio frequency-power deposition may raise body core temperature, especially in children [33, 41]. MR is absolutely contraindicated in patients with cardiac pacemakers, even using low field strength magnets. Because the magnetic field induces torque on ferromagnetic implants like aneurysm or surgical clips, patients with those materials should not be examined [24]. However, non-ferromagnetic implants are not dangerous. Except for old Starr-Edwards type, all heart valves can be imaged [24]. MR is also contraindicated in the presence of metal objects within the eye or near the spinal cord, cochlear implants, insulin pumps and neurostimulators connected to the patient. Attention has to be paid to shell fragments often seen in older patients. Encapsulated, these are normally not dangerous, but within the brain, chest or abdomen they may be dislocated and, thus, cause occult bleeding.

Lung cancer (see also other chapters)

Since the advent of MR, numerous studies have been performed to assess its value compared with CT in the management of patients with lung cancer [2, 10, 12, 19, 22, 36]. In T-staging, central lung cancers >10 mm can be detected even better than peripheral tumours [1, 2, 10, 29].

Fig. 2. – Pericardial invasion by tumour. T1-weighted parasagittal image, widespread invasive bronchogenic carcinoma with disruption of the anterior pericardial fat layer by low signal intensity tumour (arrow), widening of the pericardial space due to malignant effusion (star). Note additional tumorous chest wall invasion (arrowhead).

In assessing the tumour spread, there is good contrast between malignant soft tissue and signal void vessels or bronchi, intense mediastinal fat, and the mediastinal pleural margins. The unaltered pericardium is routinely displayed, identifiable as a line of hypointensity around the heart and the base of the major vessels, itself surrounded by a small fat plane [19, 33]. Obliteration of the mediastinal fat planes, compression, encasement or involvement of mediastinal vessels are better demonstrated by MR than by CT [2, 19, 36] (fig. 2).

In our experience, aortic tumour invasion is suggested if: 1) disruption of the periaortic fat layer of more than 90° of the circumference is present; 2) disruption of the periaortic fat is visible more than 3 cm contiguously in the cranio-caudal direction; and 3) focal disruption of the periaortic fat is visible, including deformation of the lumen [12, 19] (fig. 3). Furthermore, in selected cases focal enhancement of the aortic wall after contrast in the area of adjacent tumour tissue may indicate malignant invasion. Coronal or sagittal MR images are extremely valuable in determining the precise extent of the tumour, especially in relation to the carina and the aorto-pulmonary window, as well as in relation to the pulmonary arteries and veins. Involvement of the superior vena cava can be clearly appreciated, and, in case of significant obstruction, typical intraluminal thrombus with increased SI may be seen (fig. 4). Contrast-enhanced CT and MR are both accurate in detecting hilar masses and adenopathy [2, 19, 47, 50]. In cases of proximal bronchial obstruction associated with postobstructive pneumonitis, MR may differentiate the obstructing mass from adjacent lung on T2-weighted or contrast-enhanced T1-weighted images [1, 2, 10, 12–14, 25, 29] (fig. 5). In such patients the consolidated lung typically exhibits a higher SI than the central hilar mass. MR may even be successful in cases where differentiation is not possible with dynamic enhanced CT scanning.

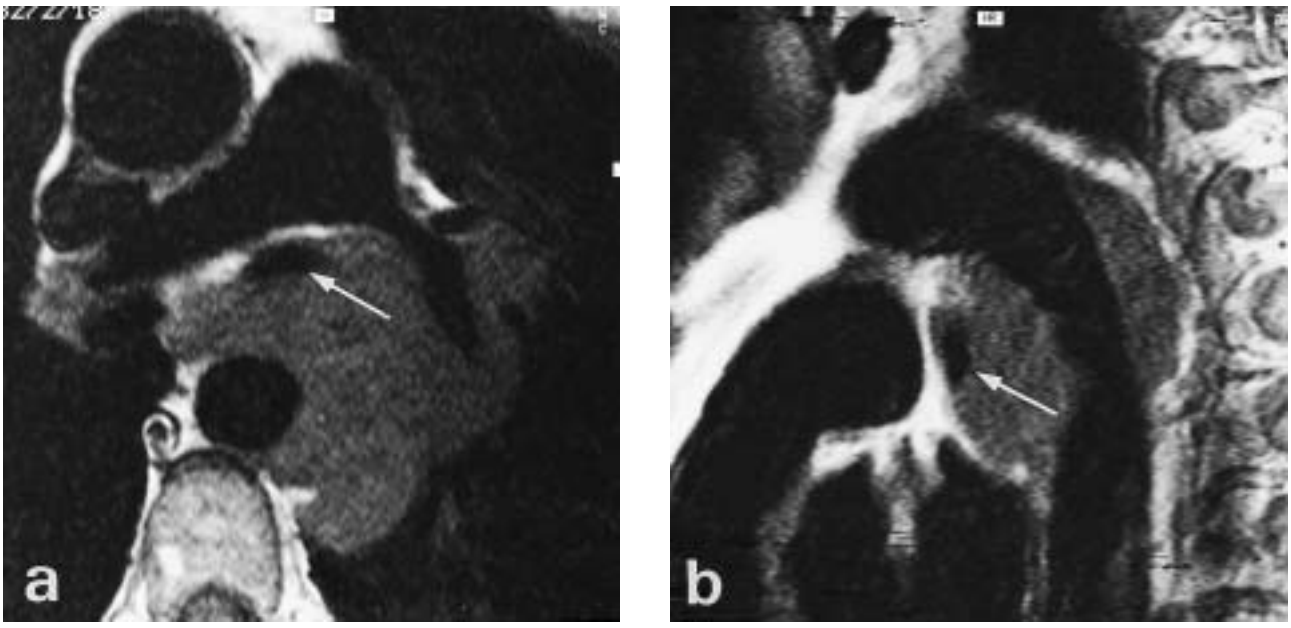

Fig. 3. – Tumourous aortic invasion. a) Transverse and b) sagittal T1-weighted magnetic resonance images demonstrate broad tumour invasion of the aortic wall by adjacent lung cancer. The perivascular fat layer has disappeared more than 180° of the circumference and more than 2 cm contiguously in the course of the aorta. In addition, mediastinal tumour invasion causes obstruction of the left pulmonary artery, as well as of the anteriorly displaced left main bronchus (arrows).

Fig. 4. – Thrombosis of the vena cava, T1-weighted coronal image. Mediastinal lymph node metastasis (arrow) due to bronchogenic carcinoma (not visible) causes occlusion of the superior vena cava with resulting intense thrombus reaching up into the jugular vein (arrowheads).

In peripheral carcinomas, contact with the pleura may suggest malignant involvement of the pleura, or of the adjacent chest wall. A thin layer of extrapleural fat separating the tumour mass from the chest wall can almost always be seen on high quality or high-resolution MR images [8, 9, 11, 31]. In such cases contrast enhanced T1-weighted MR is superior to CT in the demonstration of malignant involvement. This is especially true in superior sulcus invasion, where CT is often equivocal, due to partial volume effects (fig. 6). Sagittal or coronal plane images often show the extent of chest wall invasion and involvement of the subclavian artery or brachial plexus better than either transaxial CT or MR images [8, 9]. In patients who underwent radiation therapy for treatment of carcinoma, recurrent tumour within radiation-induced fibrosis can be difficult to identify with CT. MR has the ability to differentiate tumour from fibrosis [2, 19]. By means of high SI on T2-weighted images tumour relapse can be distinguished from post-treatment fibrosis with low SI. However, inflammatory reactions secondary to radiation or from other causes may also show increased SI on T2-weighted images.

Mediastinal masses

Generally, the relationship between a mediastinal mass and adjacent vessels and a vascular compression or obstruction is better demonstrated by MR than by contrast-enhanced CT, despite optimized contrast application with spiral CT [2, 12, 19, 36, 46–48]. The differentiation of tumour and mediastinal fat on T1-weighted MR is easy, since fat shows higher SI on T1-weighted images. However, tumour and mediastinal fat may be difficult or impossible to distinguish on T2-weighted images. The diagnosis of a mediastinal mass or an enlarged lymph node does depend on the spatial resolution and, even more important, on the soft tissue contrast resolution. MR spatial resolution is only slightly less than that of the fourth generation CT scanners, while the soft tissue contrast resolution is far better than

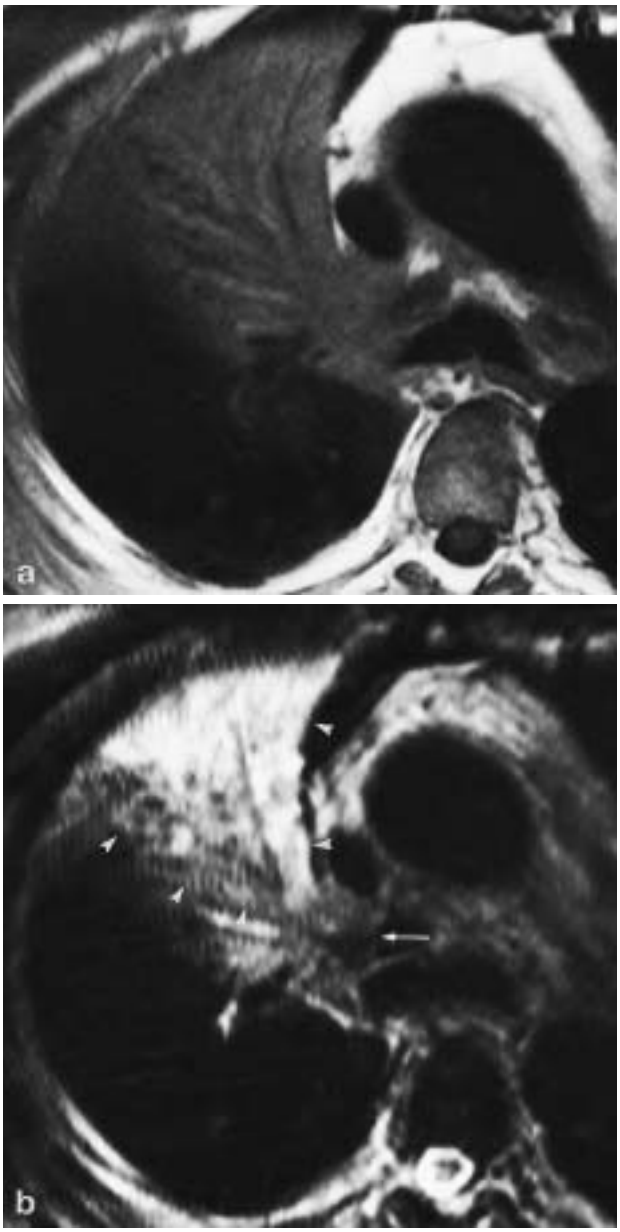

Fig. 5. – Postobstructive atelectasis. a) Unenhanced transverse T1-weighted magnetic resonance image in right central bronchogenic carcinoma, causing atelectasis of the middle lobe. There is no reliable distinction of tumour and parenchymal changes. b) Corresponding T2-weighted image with relatively low signal of centrally located tumour (arrow) and easily appreciable postobstructive atelectasis with high signal intensity (arrowheads).

that of CT [12, 19, 36]. The accuracy of both MR and CT in diagnosing mediastinal lymph node metastases, *i.e.* in patients with lung cancer, is comparable, since lymph node size is the sole criterion for determining tumour involvement [2, 19, 22, 36] (fig. 7). It is recommended that short axis of subcarinal lymph nodes should not exceed 11 mm, 10 mm for right tracheobronchial, right paraoesophageal, low paratracheal, and aorto-pulmonal, and 7–8 mm for all other nodal groups, according to the American Thoracic Society system [22, 54]. Neither relaxation times, nor SI, nor the degree of contrast enhancement are reliable indicators of malignant involvement [10, 12, 22]. However, in-

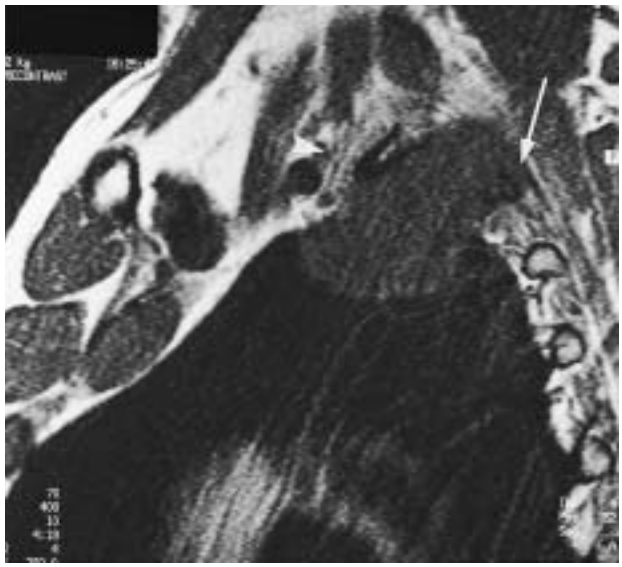

Fig. 6. – Pancoast tumour. Left-sided sagittal T1-weighted magnetic resonance image accurately displays tumour extension in Pancoast bronchogenic carcinoma with respect to superior sulcus structures. The tumour has invaded the second rib (arrow), reaches the first rib and is already adjacent to the lower fascicles of the brachial plexus, represented by linear structures behind the cross-sectional displayed left subclavian artery (arrowhead).

tense contrast enhancement of mediastinal lymph nodes in MR suggests a limited number of differential diagnoses including Castleman's disease, angioimmunoblastic lymphadenopathy, as well as vascularized metastases, in particular, from renal cell carcinoma, papillary thyroid carcinoma, and especially small-cell lung carcinoma [10, 12]. Furthermore, considerable contrast enhancement may be observed in granulomatous disease such as tuberculosis or sarcoidosis, and in acquired immune deficiency syndrome (AIDS)-related diseases, particularly Kaposi's sarcoma [3, 12, 26]. Since the presence of calcifications in a mass may be used as evidence of benign disease, a significant disadvantage of thoracic MR is that calcifications within a mediastinal mass or a node are not sufficiently detectable (fig. 8). On the

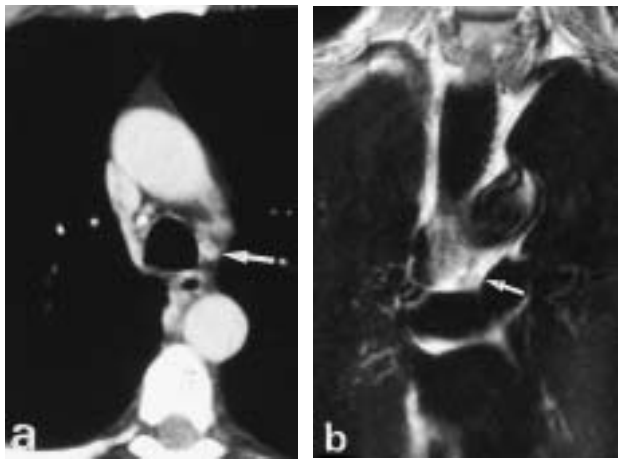

Fig. 7. – Aorto-pulmonary lymph nodes. a) Thin-section computed tomography with good contrast bolus, suspicion of small mediastinal lymph nodes, partially calcified, in the level of the aorto-pulmonary window (arrow). b) Coronal T1-weighted magnetic resonance image clearly demonstrates three small lymph nodes without partial volume effects (arrowhead).

other hand, in some cases, particularly when the aorto-pulmonary window or the subcarinal space are involved, MR is able to demonstrate lymph nodes better than CT because of its ability to image variable planes (fig. 7).

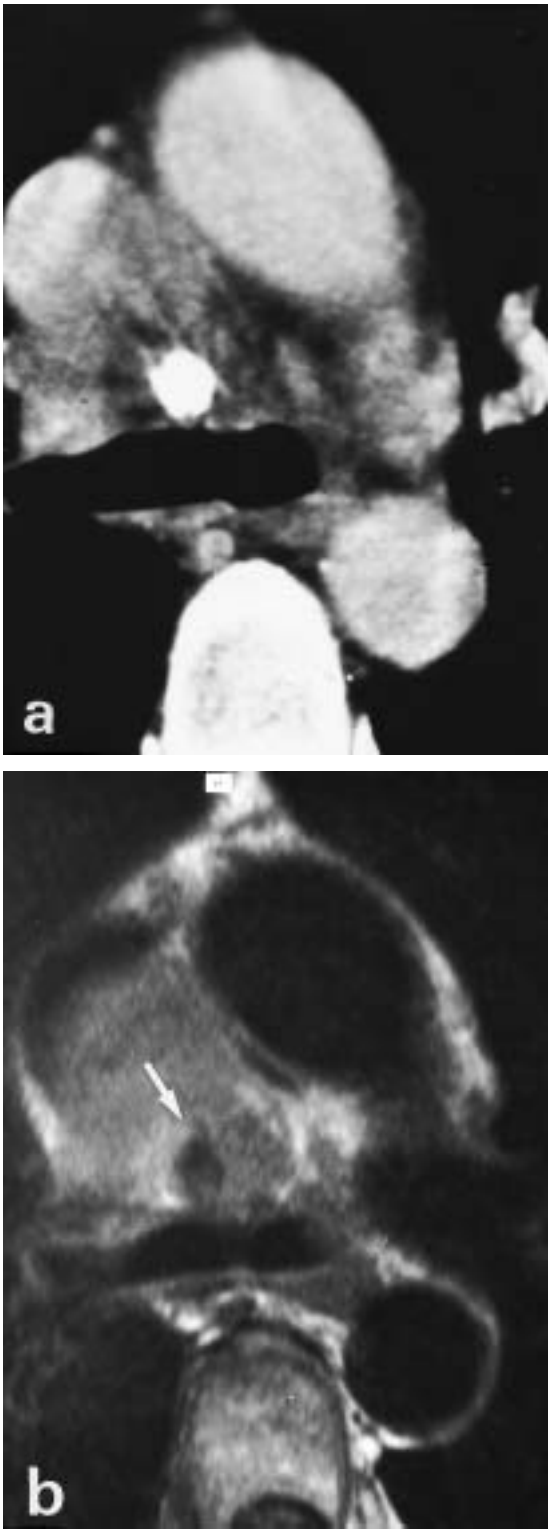

Fig. 8. – Calcified mediastinal lymph node. a) computed tomography shows large calcification in a pericarinal lymph node in a patient with multiple mediastinal and hilar metastases due to breast carcinoma. b) Corresponding transverse T1-weighted magnetic resonance image allows only suggestion of calcification due to signal-void in this region (arrow).

Regarding evaluation of the thymus, MR is comparable with CT [12, 38]. On T2-weighted images, visualization of the normal gland is more difficult than on T1-weighted images [33]. However, mediastinal thymolipoma can be diagnosed by signal characteristics due to the fat content. In patients with myasthenia gravis, no specific changes of the thymus can be seen [33]. In patients with malignant diseases, very often a thymic rebound phenomenon is visible on sagittal mediastinal T1-weighted images. On MR images, mediastinal solid thymomas characteristically present with sharply defined margins, triangular contours, with medium SI on T2-weighted images and none to slight enhancement on T1-weighted images after contrast [12].

In most cases of lymphoma, the CT density of fibrous and active lymphomatous tissue shows no significant difference, even after sufficient intravenous contrast application. Lymphomatous cells with larger amount of water show a relatively lower proportion of protein. Conversely, fibrosis contain much less water and a high proportion of protein. This leads to the markedly different T2 appearance of lymphoma and fibrosis in MR images. In nodular-sclerosing Hodgkin's disease (HD), a substantial amount of sclerosis can be seen interspersed with malignant cells. Conversely, in diffuse non-Hodgkin's lymphoma (NHL), many more malignant cells and fewer interspersed fibrous tissues may be found. Thus, characteristic signal patterns for lymphomas on T2-weighted MR images can be defined as follows:

1) A homogeneous or homogeneously fine-nodular hyperintense pattern is characteristic for untreated nonsclerosing lymphoma [12, 19]. In T1-weighted images those masses show a homogeneous low SI similar to muscle.

2) A mixed hyper-/hypointensity pattern is often seen in untreated nodular-sclerosing HD, where low-signal areas

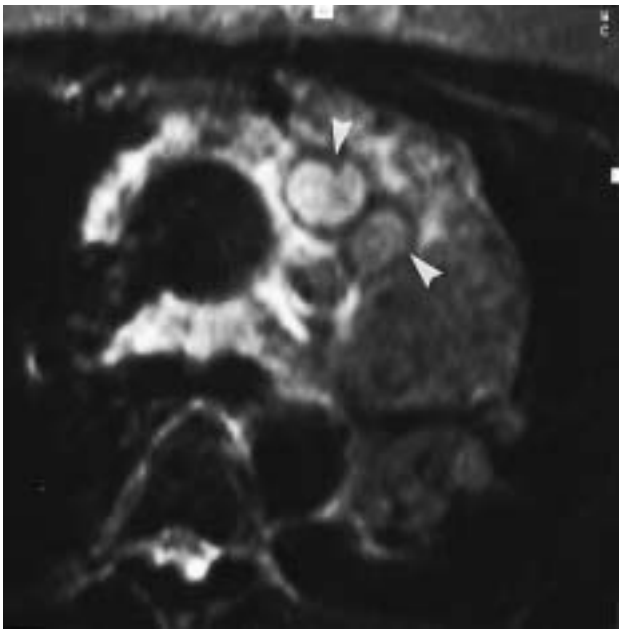

Fig. 9. – Hodgkin's disease, nodular-sclerosing type. Transverse T2-weighted image shows inhomogeneous signal intensity with ring-shaped low-signal fibrosis (arrowheads); typical appearance of nodular-sclerosing Hodgkin's lymphoma.

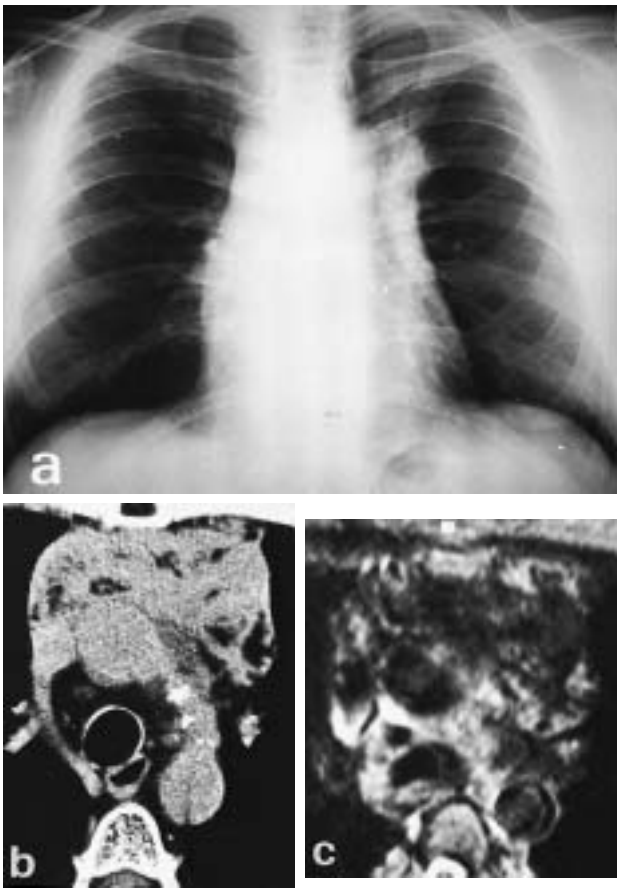

Fig. 10. – Residual mass in malignant non-Hodgkin's lymphoma. a) Chest radiograph; and b) computed tomography (CT) show extended soft tissue in the anterior mediastinum after chemotherapy and radiation of malignant B-cell lymphoma. Differentiation of fibrosis and tumour relapse is not possible. c) Corresponding (to CT) transverse T2-weighted magnetic resonance (MR) image displays fibrosis nearly signal-void, interspersed fat with higher signal intensity (SI) corresponds with low attenuation values in CT and high SI in T1-weighted MR (not shown). High SI is due to flow phenomena in the anterior azygos vein and fluid in the upper retroaortic pericardial recess.

represent sclerotic tumour regions, nodular configuration may also be found [12, 19] (fig. 9). In addition, this pattern is seen during the response phase of most lymphomas under treatment, representing residual tumour and necrosis or inflammation beside fibrosis. Mixed fibro-fatty masses are easy to recognize on T1-weighted images, since the fat portions will exhibit high SI.

3) Hypointense patterns are characteristic for inactive residual fibrotic masses following successful therapy for lymphoma and may be seen in up to 88% of patients [33] (fig. 10). These lesions also show low SI on T1-weighted images.

Thus, monitoring of SI in lymphomas by MR can contribute to therapeutic management: a decrease in mass size and a corresponding SI decrease presume a favourable response. A decrease in size with persistent homogeneous/heterogeneous hyperintense patterns suggest a partial response. Marked size regression with small residual masses of heterogeneous/homogeneous high SI strongly suggests inappropriate response of the tumour parts. SI increase within small "islands" in residual masses previously considered inactive suggests tumour recurrence. Nevertheless, cautious interpretations should be made within the first 6 months following therapy as regards inflammation and necrosis [19].

Cystic or fluid-filled masses, or necrotic changes can be detected by means of low SI on T1- and high SI on T2-weighted images, even when CT numbers suggest solid masses [19]. Detection of cystic or fluid-filled masses can also be made on the basis of no or minimal enhancement after contrast [10]. Thus, MR can be successfully used to diagnose a wide range of lesions, including bronchogenic cysts, pericardial cysts, thymic cysts, colloid cysts within goiters, dermoid cysts, cystic hygromas, and even mediastinal pseudocysts, especially complex cysts that do not appear fluid-filled on CT.

The typical MR appearance of both benign and malignant neurogenic tumours includes slightly greater SI than muscle on T1-weighted images, and moderately to markedly increased SI on T2-weighted images. Compared with CT, MR has several distinct advantages for imaging paraspinal neurogenic tumours [12, 39]. Intraforaminal/spinal extension can be clearly assessed, as well as associated spinal cord pathology [39]. Coronal or oblique sagittal images may help to assess the relationship to the sympathetic nerve. The detection of tumour infiltration beyond the parietal pleura suggests malignancy of a neurogenic mass [8, 10].

Midsagittal MR images can reliably demonstrate cranio-caudal tumour extent in patients with oesophageal carcinoma in presurgical evaluation, and suspected tumour invasion of adjacent structures can be confirmed or excluded with great sensitivity [19] (fig. 11).

Fig. 11. – Oesophageal carcinoma. Midsagittal T1-weighted image demonstrates direct cranio-caudal extent of oesophageal tumour (arrowheads). Note the unaffected normal oesophagus with slightly widened lumen below the tumorous changes.

Hilar abnormalities

The diagnosis of a hilar mass on CT images requires differentiation of normal or vascular tissue from abnormal soft tissue. In some locations, these differentiations can be made on anatomical grounds alone, but in other areas mass and vessels may be difficult to distinguish unless a precise time-controlled or large bolus of contrast medium is given. However, despite the introduction of spiral CT, in a significant number of cases the differentiation of mass and vessels after contrast is inadequate [2, 36, 47]. This problem can be avoided by using MR. Since only the walls of pulmonary arteries and veins are visible on regular T1-weighted MR images, hilar masses are easy to detect. In particular, sagittal images provide excellent spatial resolution of the hilar architecture and can detect normal size or enlarged lymph nodes [2, 19, 36].

In patients with malignant disease, contrast-enhanced CT and MR are both quite accurate in detecting hilar masses or node enlargement, with a sensitivity approaching 100% [2, 19, 36, 47, 50]. On the other hand, specificity in the detection of lymph nodes harbouring metastases, such as in the mediastinum, is rather poor using either method [22, 54]. Unfortunately, MR is unable to detect nodal calcification. On the other hand, in patients with poor vascular opacification in CT, MR allows a more confident diagnosis of a normal or abnormal hilum. In general, bronchi are more accurately evaluated with CT. MR may be advantageous in showing significant hilar or mediastinal vascular invasion contiguous with the hilar mass, and in precisely displaying its extent [2, 19, 36].

Hilar masses, *i.e*. bronchogenic carcinoma, and adjacent pulmonary obstructive collapse can be distinguished with MR [2, 14, 19, 25, 36]. Generally, tumour tissue presents with higher SI than distal lung tissue in T2-weighted images. Conversely, in tumour obstruction, distal consolidated lung parenchyma appears more intense than the tumour.

Parenchymal lung diseases

On spin-echo images in normal subjects, little signal is obtained from the lung parenchyma, mainly because of the small number of protons, magnetic susceptibility effects and the very short T2-relaxation time of lung parenchyma [41]. Fine linear structures extending laterally from the hilum into the lung represent the walls of vessels and/or bronchi. Increased SI in the parenchyma itself, often visible in the posterior area of both lungs, may represent condensation of the lung parenchyma in a supine position and an increase of intravascular blood. This signal is increased considerably after intravenous application of contrast material. Because of the signal void of normal lung parenchyma, abnormalities (nodules, masses, parenchymal changes) are easily detectable within the lungs. However, because of the invisibility of the usual structures like segmental bronchi and vessels, it may be difficult to determine the precise location of a pathological process. Nevertheless, the normal fissures are reliably displayed on sagittal images [3]. It has been shown that routine MR with 8 mm sections from the apex to the adrenals is able to successfully depict pulmonary nodules greater than 5 mm, given adequate patient compliance [2, 19, 36]. Altogether, CT is superior to MR in the diagnosis of parenchymal lung disease. Lung nodules greater than 1 cm are shown in both MR and CT, but the morphological characteristics of a nodule, such as edge definition, spiculation, and associated pleural tail are better defined with CT [4, 46, 47, 50]. Unfortunately, the presence of calcification in a nodule, important in distinguishing benign and malignant disease, is only reliably visible in thin-section or high-resolution CT (fig. 8). Overall, MR is less sensitive than CT in detecting lung nodules <1 cm in diameter, mostly due to respiratory motion during the MR study. However, in centrally-located nodules, MR may be superior to CT in distinguishing these processes from vessels [2, 19]. In pulmonary consolidation, fluid replaces air within the lung parenchyma. MR may be able to characterize the fluid or the cause of consolidation and, thus, may be able to distinguish diseases. Nonobstructive atelectasis shows a poor signal in T2-weighted images and only minimal enhancement after contrast [10, 25].

New fast sequences allow for better evaluation of interstitial lung changes, as well as cine-images of the breathing lung with the moving diaphragm and chest wall during controlled inspiration and expiration in patients with bullous emphysema and possible surgical therapy [1, 21, 29, 41]. Although spiral CT provides excellent 3D-visualization of pulmonary lesions, vascular abnormalities within the lungs like arteriovenous malformations in Osler disease are displayed by MR angiography with great accuracy [4, 17, 51].

Pleura and chest wall

Pleural and chest wall abnormalities can occur in a number of benign and malignant diseases, *e.g*. tuberculosis, asbestosis, malignant mesothelioma, lung cancer, or metastatic disease. Due to the excellent soft tissue contrast, improved spatial resolution, and imaging in various planes, MR has been proven to be especially suitable for the evaluation of pleural and chest wall abnormalities [8–11, 15, 31, 37].

Although some correlations have been found both *in vitro* and *in vivo* between MR SI and pleural fluid composition, MR cannot differentiate between various aetiologies of pleural effusions, but can distinguish free and loculated effusions, as well as identify coexistent underlying lung disease [9, 11, 31]. An accurate demonstration of pleural fluid composition is difficult with MR, but blood in the pleural space is distinguishable from other fluids, except for acute bleeding [41].

CT diagnosis of pleural disease is based on the finding of pleural effusion and pleural thickening, but the distinction of pleural and lung parenchymal abnormalities from pleural effusion may be difficult [9]. Although CT studies could demonstrate some progress in distinguishing malignant from benign pleural diseases, the infiltration of the chest wall, together with osseous destruction, still remains the only reliable sign of malignancy [9]. Recent results of MR examinations in patients with different pleural and chest wall diseases could demonstrate that MR can be extremely advantageous in these cases, improving both quality of evaluation and differential diagnosis [8, 9, 11, 15]. MR detects pleural diseases with high sensitivity, comparable with CT, and has a reliable potential in differential diagnosis of pleural changes, based on the improved

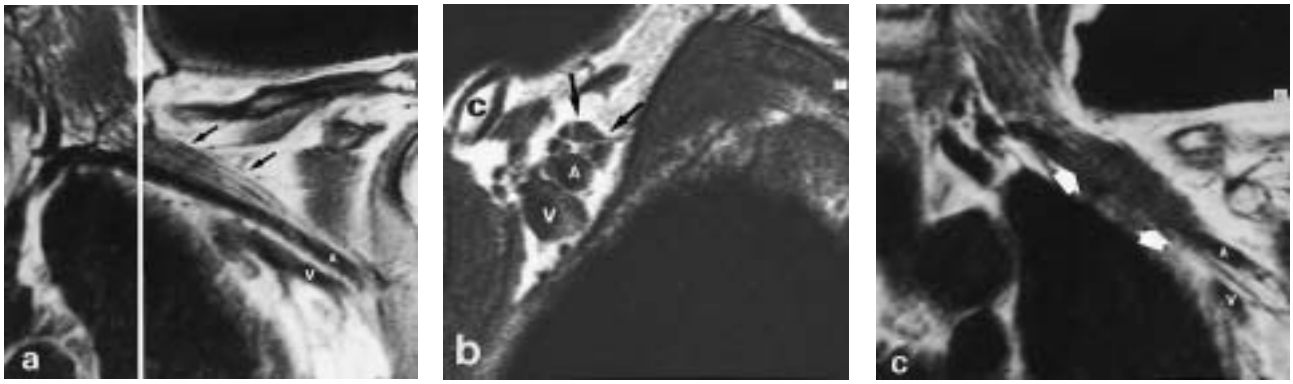

Fig. 12. – High-resolution anatomical magnetic resonance (MR) visualization of the brachial plexus. a) Oblique coronal T1-weighted MR image with typical appearance of the band-shaped fascicles of the brachial plexus (arrows) extending superiorly to the (left) subclavian artery (A) (V: subclavian vein). b) Cross-sectional sagittal view (according to the white line in (a)); behind the clavicle (C) the low-signal fascicles of the brachial plexus (arrows) are easily appreciable within the fat superior to the subclavian artery (A) and vein (V). c) Tumour invasion of the brachial plexus. Oblique coronal T1-weighted MR image shows low-signal tumour tissue of the metastatic breast cancer invading the fascicles of the plexus (arrows) and presumably involving the adjacent left subclavian artery (A).

distinction of pleural changes and adjacent structures after contrast enhancement [9, 11]. On the basis of morphological patterns such as nodular changes, thickening >10 mm, mediastinal or circumferential pleural involvement, or pleural extension through the entire hemithorax, malignant disease is suggested [9, 11]. The most specific pattern for malignancy is the infiltration of the chest wall and/or the diaphragm. MR, especially when contrast-enhanced, has demonstrated its superiority over CT in the diagnosis of diaphragm and chest wall invasion in patients with different pulmonary masses, although spiral CT has regained some ground [45]. Particularly in tumours of the superior sulcus or the lung base, images in the coronal or sagittal plane can be used to demonstrate the relationship of the tumour within the lung apex to adjacent structures such as the brachial plexus, and the subclavian artery and vein [2, 8–11, 15, 37] (fig. 6). The normal and pathological appearance of the brachial plexus is well demonstrated by T1-weighted MR images, especially regarding displacement and encasement/infiltration of the subclavian artery by tumour (fig. 12). Invasion of the diaphragm can be visualized by contrast enhancement of the regions involved [8–11] (fig. 13). The invasion of the thin layer of extrapleural fat by tumour tissue is a reliable criterion for early invasion of the chest wall [11, 15]. This fat layer is more difficult to visualize using CT.

While on unenhanced T1-weighted images tumour tissue can be easily distinguished from fat, the T2-weighted

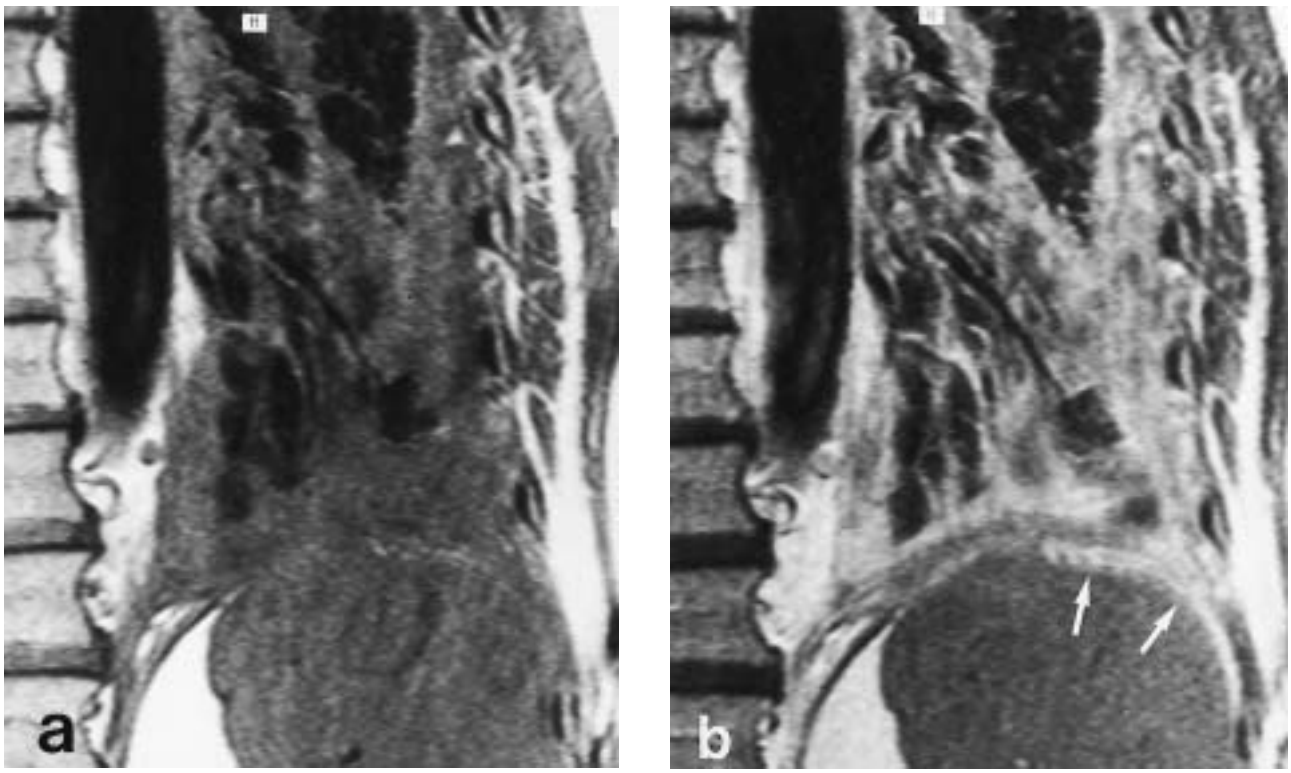

Fig. 13. – Tumour invasion of the diaphragm. a) Unenhanced and b) contrast-enhanced coronal T1-weighted magnetic resonance images in malignant pleural mesothelioma show intense band-shaped enhancement of the lateral diaphragm (arrows), representing tumour invasion (surgically confirmed).

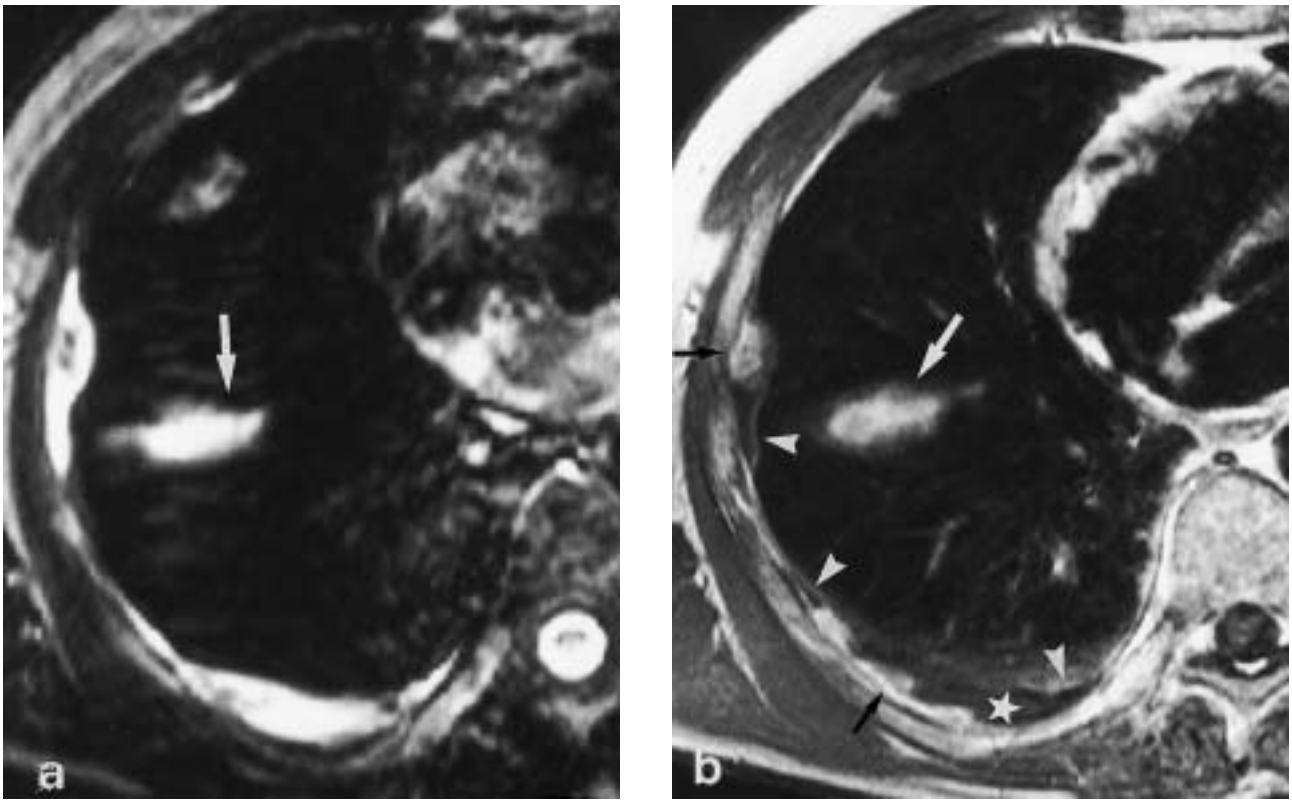

Fig. 14. – Primary pleural liposarcoma. a) Transverse T2-weighted magnetic resonance image displays pleural and fissural (arrow) changes with high signal intensity. No reliable distinction of pleural effusion and tumourous changes. b) Corresponding contrast-enhanced T1-weighted image. Excellent differentiation of enhancing irregularly defined parietal tumour nodules (black arrows), non-enhancing effusion (star), slightly thickened visceral pleura (arrowheads), and fissural tumour involvement (white arrow).

and contrast-enhanced T1-weighted image allow reliable distinction of tumour and muscle. Contrast-enhanced T1-weighted images are superior to T2-weighted images because of their improved spatial resolution with comparable lesion contrast [8–11]. Therefore, and because of the absolute increase in signal within the pleural space in the presence of pleural changes on T2-weighted images, the method of choice in pleural MR should be unenhanced and contrast-enhanced T1-weighted sequences (fig. 14). Improved imaging of pleural pathology and chest wall invasion is achieved by using surface coils. High-resolution MR studies of the pleural space and the inner chest wall suggest a reliable approach in the differential diagnosis of pleural diseases, and in the early detection of malignant chest wall invasion [9, 11] (fig. 15).

Vascular lesions, heart and pericardium

MR imaging has proven valuable in the diagnosis of a number of vascular changes involving the mediastinum [12, 16, 18–20, 34, 35, 43]. Aortic aneurysms are easily identified with MR because of the signal void usually associated with flowing blood. Organized thrombi within the lumen of aneurysms usually appear as areas of intermediate to increased SI on T1-weighted images. T1-weighted MR may be limited in differentiating between mediastinal fat and subacute or chronic haemorrhage because of a leaking aneurysm, owing to potential overlap in their SI parameters [33–35]. MR and spiral CT are used equally in screening for aortic dissection [47, 53]. ECG-gated T1-weighted spin-echo sequences, best acquired in transverse and coronal/sagittal planes, can demonstrate intimal flap in patients with dissection, with an accuracy equalling or exceeding that of CT [34, 35].

In patients with superior vena cava obstruction, the area of narrowing or obstruction can be demonstrated [2, 12, 19, 33, 36]. Furthermore, the evidence of slow flow is seen, and increased SI within the lumen of the superior vena cava suggests the diagnosis of thrombosis [19] (fig. 4). However, a fresh thrombus may appear similar to flowing blood and may be missed on unenhanced or nonangiographic MR images [33, 41]. Contrast-enhanced MR is able to differentiate thrombus from intravascular tumour [10, 12]. On MR angiographic images, central emboli are displayed as low intensity defects within the high signal of flowing blood [6, 20] (fig. 16). Nevertheless, in pulmonary artery embolism, to date, spiral CT with bolus-application of contrast material is the method of choice [4, 20, 35, 44, 47, 49, 53]. In patients with tumour involvement of the main pulmonary arteries or veins, MR can better demonstrate the tumorous extension, compared with CT [2, 12, 19, 36, 43].

In the evaluation of the heart and the pericardium, the advantages of MR include larger FOV than ultrasound and far better soft-tissue contrast resolution than ultrasound and CT. While cine-MR is believed to be the most sensitive method for detecting pericardial effusion and intracavitary masses, myocardial and pericardial masses are best imaged with spin-echo techniques [2, 12, 16, 18, 23, 24,

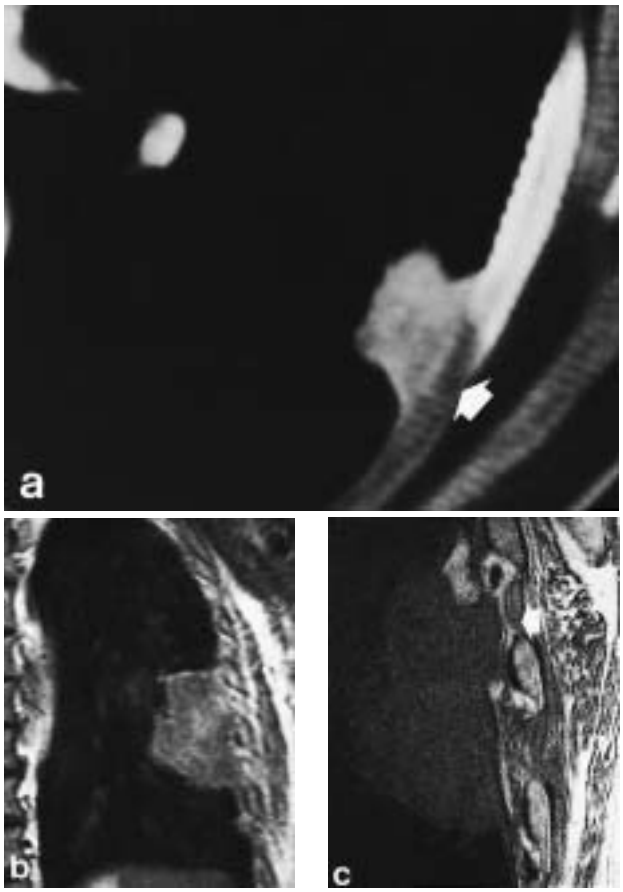

Fig. 15. – Malignant invasion of the chest wall. a) Computed tomography shows pleura-based tumour mass with broad contact to the intercostal soft tissue and presumable invasion (arrow). b) Conventional coronal T1-weighted magnetic resonance (MR) image demonstrates broad tumour contact with the lateral chest wall. c) High-resolution sagittal T1-weighted MR image excellently reveals focal invasion of the inner chest wall with disruption of the peripleural fat, involvement of the innermost intercostal muscle and the intercostal fat (arrow). Surgery confirmed focal chest wall invasion by malignant fibrous histiocytoma.

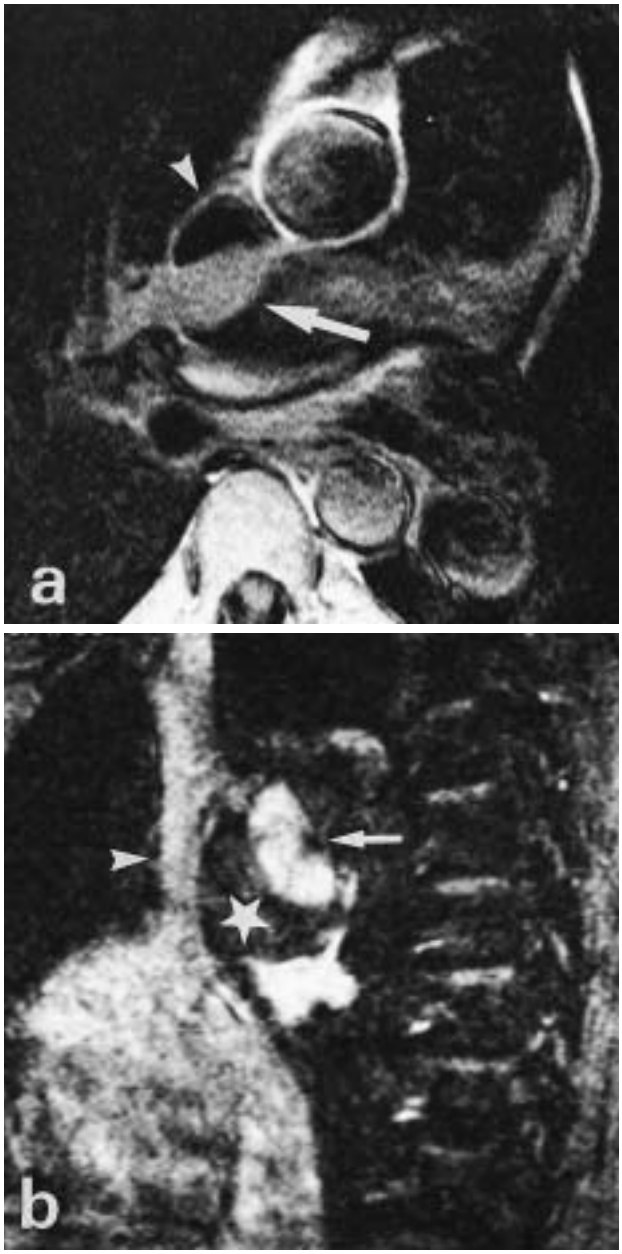

Fig. 16. – Pulmonary artery thrombosis. a) T1-weighted transverse image shows low-signal thrombus adjacent to the anterior vascular wall (arrow) with compression of the lumen of the superior vena cava (arrowhead). b) Parasagittal magnetic resonance-angiogram demonstrates nearly signal-void thrombus (star), high-signal true lumen of the enlarged right pulmonary artery (arrow), and medium-signal of the compressed superior vena cava (arrowhead).

28, 30, 43]. MR is particularly sensitive for the presence of pericardial fluid, especially intrapericardial haemorrhage [2, 19, 43]. When combined pericardial and cardiac inflammatory or tumorous involvement is suspected, MR is usually superior to CT and ultrasound [2, 12, 19] (fig. 2).

Summary

Compared with CT, the main advantages of MR are the ability to conduct multiplanar imaging, the excellent soft tissue contrast, the depiction of vascular structures without the use of contrast material, and the ability to produce detailed angiographic images of mediastinal and pulmonary vasculature, already comparable with digital substraction angiography. The the main disadvantage of MR compared with CT in clinical routine is the longer examination time, in addition to the insufficient demonstration of calcifications. MR is used as a primary imaging modality in patients with suspected vascular lesions, mediastinal masses, hilar lesions, and pathological changes of the pleura and the chest wall. In many other patients, MR is used as a problem-solving modality in answering specific questions raised by the CT study or clinical findings. Detailed information can be achieved by high-resolution MR regarding pleural and chest wall changes, especially after contrast application. MR is able to distinguish different tissues, fluids, or pathological processes within the chest. Furthermore, qualitative and quantitative data regarding blood flow, volume and blood pressure within vessels and the heart, as well as diaphragm function can be obtained. Postprocessing algorithms, which are being increasingly used, can eliminate motion, flow, breathing and other artifacts, and significantly improve MR image quality.

Future outlook

About 15 years after the introduction of magnetic resonance imaging into clinical routine, there are emerging applications expanding magnetic resonance from a purely diagnostic modality to its use in guiding invasive procedures throughout the body. Dedicated interventional magnetic resonance-systems with open magnets are being developed, allowing direct access to patients during procedures such as magnetic resonance-endoscopy, stereotactic biopsy, radiofrequency tumour ablation, or laser discectomy. Magnetic resonance-guided-biopsy and laser-induced interstitial thermotherapy has already been established in liver, breast and neck abnormalities. In pretherapeutic planning three-dimensional-image reconstruction and "virtual reality" processing of simulated vascular, intestinal and bronchial endoscopies, as well as simulated surgical interventions, are being developed. Real-time magnetic resonance techniques allow for reliable functional imaging comparable with ultrasound, and tissue temperatures can be noninvasively measured and also used for thermal imaging.

References

1. Alsop DC, Hatabu H, Bonnet M, Listerud J, Gefter W. Multi-slice, breathhold imaging of the lung with submillisecond echo times. *MRM* 1995; 33: 678–682.
2. Armstrong P, Reznek RH, Phillips RR. Diagnostic imaging of lung cancer. *In*: Spiro SG, ed. Carcinoma of the Lung. *Eur Respir Mon* 1995; 1: 137–187.
3. Auffermann W, Hieckel HG, Bittner RC, *et al*. Magnetresonanz-Tomographie der Lunge bei pulmonaler Sarkeidose. *Pneumologie* 1992; 46: 277–281.
4. Beier J, Liebig T, Bittner RC, *et al*. Computergraphische Methoden zur dreidimensionalen Darstellung intrapulmonaler Raumforderungen aus CT- und MR-Bildern. *Pneumologie* 1996; 50: 672–678.
5. Beier J, Bittner RC, Wust P, Fleck E, Kaiser D, Felix R. 3-D-Darstellung von thorakalen Tumoren aus MR-Bildern. *Fortschr Roentgenstr* 1996; 164: 75–78.
6. Bergin CJ, Hauschildt J, Rios G, Belezzuoli EV, Huynh T, Channick RN. Accuracy of MR angiography compared with radionuclide scannning in identifying the cause of pulmonary arterial hypertension. *AJR* 1997; 168: 1549–1555.
7. Berthezène Y, Vexler V, Clément O, Mühler A, Moseley ME, Brasch RC. Contrast-enhanced MR imaging of the lung: assessments of ventilation and perfusion. *Radiology* 1992; 183: 667–672.
8. Bittner RC, Kaiser D, Loddenkemper R, Felix R. Wertigkeit der Magnetresonanztomographie bei Pancoast- und anderen Tumoren mit Infiltration der Thoraxwand. *Pneumologie* 1990; 44: 62–69.
9. Bittner RC, Schoerner W, Loddenkemper C, *et al*. Pleuraerkrankungen in der Magnetresonanztomographie (MRT). *Pneumologie* 1992; 46: 612–620.
10. Bittner RC, Schoerner W, Auffermann W, *et al*. Contrast enhanced magnetic resonance imaging in chest pathologies. *Am Rev Respir Dis* 1992; 145: A196.
11. Bittner RC, Schnoy N, Schoenfeld N, *et al*. Hochauflösende Magnetresonanztomographie (HR-MR) von Pleura und Thoraxwand: Normalbefund und pathologische Veränderungen. *Fortschr Roentgenstr* 1995; 162: 296–303.
12. Bittner RC, Schoenfeld N, Loddenkemper R, Kaiser D, Dorow P, Felix R. Improved differential diagnosis with magnetic resonance imaging (MRI) in mediastinal pathologies. *Am J Respir Crit Care Med* 1995; 151: A846.
13. Bockisch A, Daniel G, Harvey RC, Davis MA, Kabalka GW. MRI contrast enhancement of the lung using a Gd-DTPA aerosol. *Radiologica Diagnostica* 1993; 34: 103–105.
14. Bourgouin PM, McLoud TC, Fitzgibbon JF, *et al*. Differentiation of bronchogenic carcinoma from postobstructive pneumonitis by magnetic resonance imaging: histopathologic correlation. *J Thorac Imaging* 1991; 6: 22–27.
15. Carlsen SE, Bergin CJ, Hoppe RT. MR imaging to detect chest wall and pleural involvement in patients with lymphoma: effect on radiation therapy planning. *AJR* 1993; 160: 1191–1195.
16. Chin AJ, Fogel MA. Noninvasive Imaging of Congenital Heart Disease. Before and After Surgical Reconstruction. New York, Futura, 1994.
17. Dinsmore BJ, Gefter WB, Hatabu H, Kressel HY. Pulmonary arteriovenous malformations: diagnosis by gradient-refocused MR imaging. *J Comput Assist Tomogr* 1990; 14: 918–923.
18. Dueriockx AJ. Coronary MR angiography. *MRI Clin North Am* 1996; 4: 361–418.
19. Felix R, Bittner RC. Wertigkeit der Magnetresonanztomographie (MRT) in der Pneumologie. *Internist* 1993; 34: 1038–1043.
20. Gefter WB, Hatabu H, Holland GA, Gupta KB, Henschke CI, Palevsky HI. Pulmonary thromboembolism: recent developments in diagnosis with CT and MR imaging. *Radiology* 1995; 197: 561–574.
21. Gierada DS, Curtin JJ, Erickson SJ, Prost RW, Strandt JA, Goodman LR. Diaphragmatic motion: fast gradient-recalled-echo MR imaging in healthy subjects. *Radiology* 1995; 194: 879–884.
22. Glazer GM, Orringer MB, Chenevert TL, *et al*. Mediastinal lymph nodes: relaxation time/pathologic correlation and implications in staging of lung cancer with MR imaging. *Radiology* 1988; 168: 429–431.
23. Hartnell GG, Cerel A, Kamalesh M, *et al*. Detection of myocardial ischemia: value of combined myocardial perfusion and cineangiographic MR imaging. *AJR* 1994; 163: 1061–1067.
24. Hartnell GG, Spence L, Hughes LA, Cohen MC, Saouef R, Buff B. Safety of MR imaging in patients who have retained metallic materials after cardiac surgery. *AJR* 1997; 168: 1157–1159.
25. Herold CJ, Kuhlmann JE, Zerhouni EA. Pulmonary atelectasis: signal pattern with MR imaging. *Radiology* 1991; 178: 710–715.
26. Khalil AM, Carette MF, Cadranel JL, Mayaud CM, Akoun GM, Bigot JM. Magnetic resonance imaging findings in pulmonary Kaposi's sarcoma: a series of 10 cases. *Eur Respir J* 1994; 7: 1285–1289.
27. Leung DA, Debatin JF, Wildermuth S, *et al*. Intravascular MR tracking catheter: preliminary experimental evaluation. *AJR* 1995; 164: 1265–1270.
28. Lombardi M. Ultrafast MR methods detect and diagnose myocardial infarction. *Diagn Imag Int* 1994; 11: 56–59.
29. Lutterbey G, Gieseke J, Sommer T, Keller E, Kuhl C, Schild H. Ein neuer Ansatz in der Magnetresonanztomographie der Lunge mit einer ultrakurzen Turbo-Spin-Echo-Sequenz (UTSE). *Fortschr Roentgenstr* 1996; 164: 388–393.
30. Masui T, Finck S, Higgins CB. Constructive pericarditis and restrictive cardiomyopathy: evaluation with MR imaging. *Radiology* 1992; 182: 369–373.
31. Müller NL. Imaging of the pleura. *Radiology* 1993; 186: 297–309.

32. Mumtaz H, Hall-Craggs MA, Wotherspoon A. Laser therapy for breast cancer: MR imaging and histopathological correlation. *Radiology* 1996; 200: 651–658.
33. Naidich DP, Zerhouni EA, Siegelman SS. Computed Tomography and Magnetic Resonance of the Thorax, 2nd edition. New York, Raven Press, 1991.
34. Nienaber CA, von Kodolitsch Y, Nicolas V, *et al*. The diagnosis of thoracic aortic dissection by noninvasive imaging procedures. *N Engl J Med* 1993; 328: 1–9.
35. Prince MR, Narasimhan DL, Jacoby WT, *et al*. Three-dimensional Gadolinium-enhanced MR angiography of the thoracic aorta. *AJR* 1996; 166: 1387–1397.
36. Quint LE, Francis IR, Wahl RL, Gross BH, Glazer GM. Preoperative staging of non-small-cell carcinoma of the lung: imaging methods. *AJR* 1995; 164: 1349–1359.
37. Rapoport S, Blair DN, McCarthy SM, Desser TS, Hammers LW, Sostman HD. Brachial plexus: correlation of MR imaging with CT and pathologic findings. *Radiology* 1988; 167: 161–165.
38. Sakai F, Sone S, Kiyono K, *et al*. MR imaging of thymoma: radiologic-pathologic correlation. *AJR* 1992; 158: 751–756.
39. Sakai F, Sone S, Kiyono K, *et al*. Intrathoracic neurogenic tumors: MR-pathologic correlation. *AJR* 1992; 159: 279–283.
40. Silverman JM, Julien PJ, Herfkens RJ, Pelc NJ. Quantitative differential pulmonary perfusion: MR imaging *versus* radionuclide lung scanning. *Radiology* 1993; 189: 699–701.
41. Stichnoth FA. MR-Tomographie. Technische Grundlagen und klinische Aspekte, 2nd edition. Berlin, Blackwell Wissenschaft, 1994.
42. Vogl TJ, Muller PK, Hammerstingl R. Malignant liver tumors treated with MR imaging-guided laser-induced thermotherapy: technique and prospective results. *Radiology* 1995; 196: 257–265.
43. Wetter DR, McKinnon GC, Debatin JF, von Schulthess GK. Cardiac echo-planar MR imaging: comparison of single- and multiple-shot techniques. *Radiology* 1995; 194: 765–770.
44. Bergin CJ, Rios G, King MA, Belezzuoli EV, Luna J, Auger WR. Accuracy of high-resolution CT in identifying chronic pulmonary thromboembolic disease. *AJR* 1996; 166: 1371–1377.
45. Brink JA, Heiken JH, Semenkovich J, Teefey SA, McClennan BL, Sagel SS. Abnormalities of the diaphragm and adjacent structures: findings on multiplanar spiral CT scans. *AJR* 1994; 163: 307–310.
46. Buckley JA, Scott WW Jr, Siegelman SS, *et al*. Pulmonary nodules: effect of increased data sampling on detection with spiral CT and confidence in diagnosis. *Radiology* 1995; 196: 395–400.
47. Heiken JP, Brink JA, Vannier MW. Spiral (helical) CT. *Radiology* 1993; 189: 647–656.
48. Kauczor HU, Wolcke B, Fischer B, Mildenberger P, Lorenz J, Thelen M. Three-dimensional helical CT of the tracheobronchial tree: evaluation of imaging protocols and assessment of suspected stenoses with bronchoscopic correlation. *AJR* 1996; 167: 419–424.
49. Kuzo RS, Goodman LR. CT evaluation of pulmonary embolism: technique and interpretation. *AJR* 1997; 169: 959–965.
50. Paranjpe DV, Bergin CJ. Spiral CT of the lungs: optimal technique and resolution compared with conventional CT. *AJR* 1994; 162: 561–567.
51. Remy J, Remy-Jardin M, Giraud F, Wattinne L. Angioarchitecture of pulmonary arteriovenous malformations: clinical utility of three-dimensional helical CT. *Radiology* 1994; 191: 657–664.
52. Vining DJ, Liu K, Choplin RH, Haponik EF. Virtual bronchoscopy: relationships of virtual reality endobronchial simulations to actual bronchoscopic findings. *Chest* 1996; 109: 549–553.
53. Beier J, Diebold T, Liebig T, Biamino G, Fleck E, Felix R. Virtual endoscopy in the assessment of aortic lesions. *AJR* 1997; 168: S178.
54. Kiyono K, Sone S, Sakai F, *et al*. The number and size of normal mediastinal lymph nodes: a postmortem study. *AJR* 1988; 150: 771–776.